



Design of Modified UWB Microstrip Antenna for UHF Partial Discharge Sensor

Umar Khayam ^{1*}, Yuda M. Hamdani ¹, Rachmawati ^{1, 2}

¹ School of Electrical Engineering and Informatics, Institut Teknologi Bandung, Bandung 40132, Indonesia.

² Research Center for Nanosciences and Nanotechnology, Institut Teknologi Bandung, Bandung 40132, Indonesia.

Abstract

The development of printable ultrahigh-frequency (UHF) antennas as partial discharge (PD) sensors for high-voltage equipment has been extensively studied. However, achieving ultrawideband (UWB) UHF PD sensors frequently requires larger sizes, unsuitable for certain applications requiring compact sensors for dielectric windows in HV equipment. This research objective is to obtain PD sensors with a wider bandwidth (0.3–3 GHz) and a compact size fitting a less-than-100mm-length gas-insulated switchgear (GIS) dielectric window. A circular patch microstrip antenna (CPMA) was chosen for its small size and potential for UWB performance. This paper discusses the design modification of the CPMA to obtain a wider bandwidth for PD detection in GIS. Simulations and lab-scale experimental verifications were conducted to evaluate the optimized sensor. The modified sensor, with a size of $60 \times 73 \text{ mm}^2$, achieved a bandwidth of 3.08–3.14 GHz, a reflection coefficient of -44 dB, and several resonant frequencies of 0.3–2.3 GHz. This is a seven-time wider bandwidth compared to earlier bowtie antennas while keeping a dimension of less than 100 mm^2 . These properties allow for efficient PD detection in GIS and other insulating media. Experimental results indicate the sensor's capacity to reliably detect and analyze PD signals while responding appropriately to variations in voltage.

Keywords:

Partial Discharge;
UHF Sensor;
Gas Insulated Switchgear;
Circular Patch Microstrip Antenna.

Article History:

Received:	14	March	2024
Revised:	28	August	2024
Accepted:	06	September	2024
Published:	01	October	2024

1- Introduction

The reliability of electrical power systems is strongly related to the power quality received at the consumers' end, with insulation failure responsible for approximately 80% of power system apparatus failures, leading to frequent power interruptions [1, 2]. Partial discharge (PD) occurrence is an early indicator of insulation degradation, which if untreated, may lead to electrical breakdown. Thus, early PD detection is crucial for the condition monitoring of the HV power apparatus [3].

Various UHF sensors with various bandwidth specifications have been developed for PD detection due to their high flexibility, contactless nature, and ability to monitor PD from a safe distance. These sensors are designed to detect PD signals that emit electromagnetic waves in the UHF range of 300 MHz – 3 GHz [4]. However, PD signals in air or oil insulation media, such as in air-insulated switchgear or power transformers, may occur at lower frequencies than UHF [5, 6]. Despite the advancements, some of the current UHF sensors designed for PD detection in HV apparatus have not achieved the desired bandwidth. Some others fulfill the operating frequency range with the cost of larger antenna dimensions. For instance, our prior designs, which include several modified bowtie antennas, had a bandwidth of less than 1 GHz, which is insufficient for comprehensive PD detection in HV power apparatus [7]. Additionally, the

* **CONTACT:** umar@itb.ac.id

DOI: <http://dx.doi.org/10.28991/ESJ-2024-08-05-03>

© 2024 by the authors. Licensee ESJ, Italy. This is an open access article under the terms and conditions of the Creative Commons Attribution (CC-BY) license (<https://creativecommons.org/licenses/by/4.0/>).

constraints of dielectric window sizes in HV equipment, such as in a 66-kV gas-insulated switchgear (GIS) and a 125 MVA 66/230 kV HV power transformers, limit the feasible dimensions of these sensors [8-10].

The difficulty lies in creating a UHF antenna with ultrawide bandwidth (UWB) that can be accommodated within these specified size limitations. The current solutions, such as spiral and fractal antennas, are either too large to be installed on dielectric windows of HV equipment or do not adequately cover the required frequency range [11-13]. Lozano-Claros et al. designed a spiral antenna with a substantial diameter of 190 mm, capable of covering a frequency range of 0.3 to 1.5 GHz [14]. Azam et al. developed a UHF planar sensor aims to reduce noise during PD detection. However, despite its smaller dimension than spiral antenna ($160 \times 80 \text{ mm}^2$), the sensor only has a bandwidth of 0.8 to 1.4 MHz [15]. Yadam et al. presented an enhanced UWB UHF tapered planar spiral (TPS) antenna with a bandwidth extension from 0.57 to 3.5 GHz. Nevertheless, the antenna's diameter of 159 mm may still be too large for some GIS dielectric windows [16]. Dhara et al. developed a wall-mounted UWB multilayered PD sensor specifically designed to be placed on the inner side of the oil tank of HV power transformer. This sensor has a frequency range of 0.3 to 3 GHz and a bandwidth of about 2.5 GHz. However, its 150 mm diameter limited its external installation flexibility [17]. In addition, Shu et al. designed a printed monopole antenna (PMA) with dimensions of $220 \times 160 \text{ mm}^2$ which exhibits low-noise and enhanced sensitivity. Despite its enhanced noise cancellation and impedance matching performance, it has limited bandwidth of 0.4 to 1.1 GHz as an external sensor for PD detection in GIS [18]. The results of these studies highlight the significant gap in creating compact UHF sensors with sufficient bandwidth to ensure accurate PD detection across various installation settings.

This research aims to address this gap by utilizing and enhancing a UWB circular patch microstrip antenna (CPMA) configuration, initially developed for Stepped-Frequency Continuous-Wave Ground Penetrating Radar (SFCW-GPR) [19], for the purpose of PD detection applications. The CPMA [19], which has a standard design bandwidth of more than 3 GHz and dimensions of less than $60 \times 73 \text{ mm}^2$, is suitable for fitting on GIS dielectric windows. Our research attempts to improve this design in order to attain a wider bandwidth in the UHF range for PD detection while preserving low reflection coefficients and higher resonant frequencies.

In this paper, a comprehensive explanation of the optimization process for the CPMA is discussed, which involves modifying dimension parameters to improve the bandwidth characteristics. Following this, the fabrication process and measurements of sensor characteristics utilizing vector network analyzers (VNA) are clarified. Finally, the effectiveness of the fabricated antennas is assessed in a high-voltage laboratory environment to detect and analyze PD signals.

2- Design and Optimization

The research methodology, as depicted in Figure 1, describes the approach by combining computer simulation with experimental verification in the laboratory.

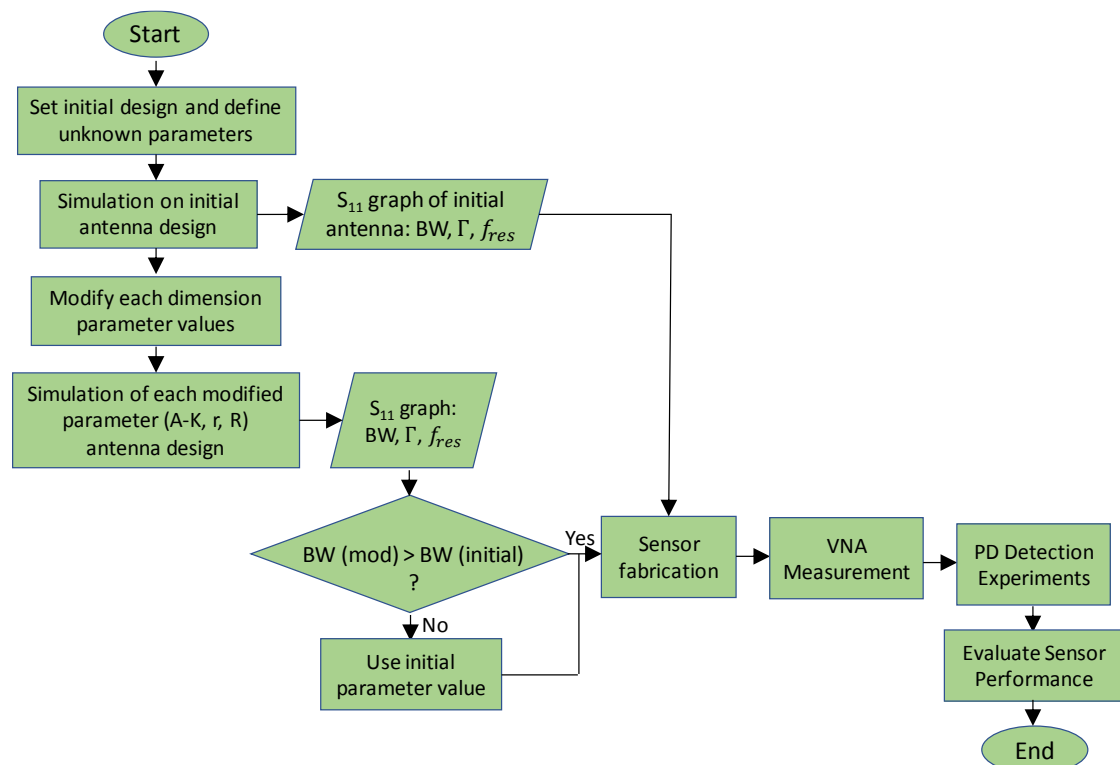


Figure 1. Flow chart of the research method

2-1-Initial Design of Modified Microstrip Antenna

Figure 2 illustrates the octopus microstrip antenna used as the reference. It consists of three primary components: the arm, the head, and the ground plane. Table 1 provides the specific values of each dimension parameter in Figure 2, which are determined from the reference design [20, 21]. The reference design (Simorangkir & Munir [20]) does not explicitly provide some dimensions; hence our study designates them as parameters: feed (H), width of arms (I), width of inner ground plane (J), and length of resistive loading (K). The specified dimensions for the initial design used in this study are as follows: H = 2 mm, I = 2 mm, J = 6 mm, and K = 3 mm.

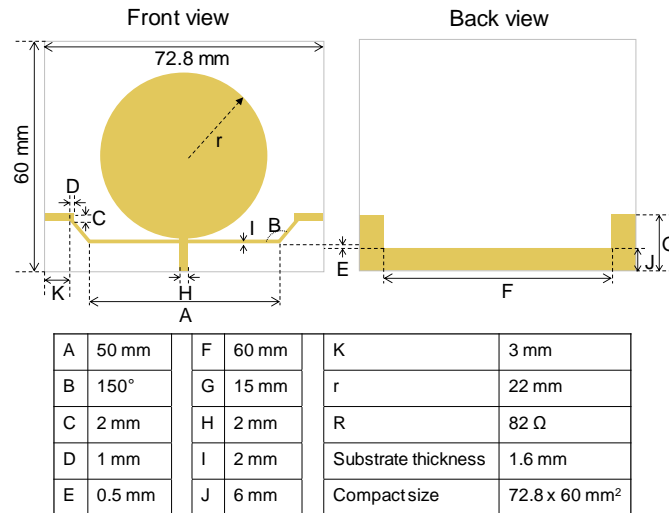


Figure 2. Initial design of modified microstrip antenna with specified dimensions

Table 1. Dimension of reference microstrip antenna [20, 21]

Parameter	Description	Value
A	Length of arms	50 mm
B	Transition angle	150°
C	Width of resistive loading	2 mm
D	Length of arms after transition	1 mm
E	Position of arms from ground plane	0.5 mm
F	Length of ground plane	60 mm
G	Width of ground plane	15 mm
H	Feed	2 mm
I	Width of arms	2 mm
J	Width of inner ground plane	6 mm
K	Length of resistive loading	3 mm
r	radius of circular patch	22 mm
R	Resistive loading value	82 Ω
	Substrate thickness	1.6 mm
	Compact size	72.8 x 60 mm ²

Subsequently, each dimension is optimized through simulations utilizing antenna design software, employing both reduced and increased values in comparison to the initial specifications. The results suggest that most of the initial design dimension parameters already yield the most optimal values for generating the widest bandwidth, which are consistent with the dimensions of the reference antenna listed in Table 1. Nevertheless, the optimal bandwidth values for dimension parameters A, F, and H exhibit differences, indicating the potential for further optimization.

The S_{11} -parameter graph in Figure 3 represents the reflection coefficients of the microstrip antenna's initial design. At resonance frequencies of 0.26 and 1.92 GHz, the reflection coefficients are -20.28 dB and -16.93 dB, respectively. The total bandwidth, defined as the range where the reflection coefficient is less than -10 dB, is 2.30 GHz.

The following subsections outline the modifications made to the arm length (A), ground plane length (F), and feed (H) dimensions. These modifications are compared to the initial design shown in Figure 2, together with the antenna characteristics shown in Figure 3.

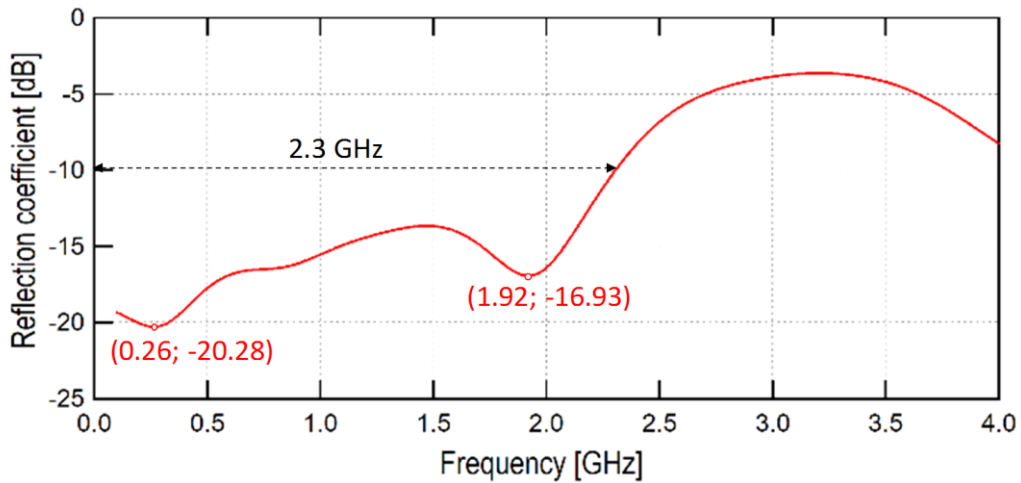


Figure 3. Reflection coefficient of the initial design of microstrip antenna

2-2-Modification of Length of Arms (A)

The first design optimization involves changing the length of arms (A in Figure 2) by using smaller and larger values of 45 mm and 55 mm, respectively, in comparison to the initial value of 50 mm. Figure 4 displays the simulation results of the reflection coefficient for various length of arms, while Table 3 presents the characteristics of the antenna. The antenna's bandwidth can be maximized by adjusting the length of arms. By using arms with lengths of 45 mm and 55 mm, the antenna with 55-mm arms achieves the widest bandwidth of 2.39 GHz. This is different from its initial length of 50 mm

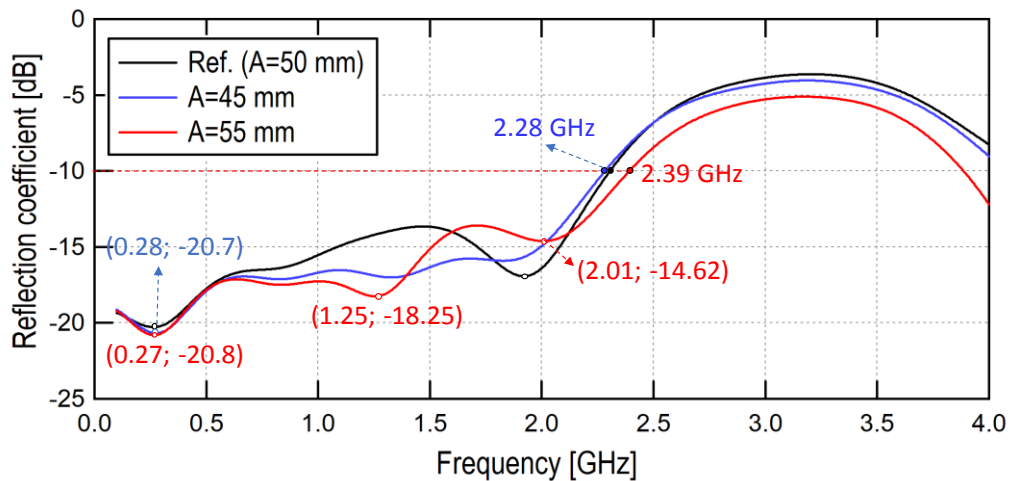


Figure 4. Reflection coefficient of the modified microstrip antenna with a length of arms (A) of 45 mm, 50 mm, and 55 mm

Table 2. S₁₁ parameter simulation results of varying length of arms (A)

Length of Arms [mm]	Bandwidth [GHz]	Reflection Coefficient Γ [dB]	Resonance frequency [GHz]
45 mm	2.28	-20.7	0.28
50 mm [ref.]	2.30	-20.28, -16.93	0.26, 1.92
55 mm	2.39	-20.8, -18.25, -14.62	0.27, 1.25, 2.01

2-3-Modification of Length of Ground Plane (F)

Secondly, the modification of the microstrip antenna's dimensions that results in improved bandwidth compared to the initial value can be achieved by modifying the length of the ground plane (F in Figure 2). The initial value of F is 55 mm. Then, both smaller and larger values of F were tested, specifically with F=50 mm and 65 mm.

Figure 5 presents the S₁₁ parameter simulation results for the modified F values with the corresponding bandwidth, reflection coefficient, and resonance frequency provided in Table 3. The results indicate a trend where increasing the width of resistive loading leads to a decrease in bandwidth and resonant frequency, along with a slight reduction in the reflection coefficient. The maximum bandwidth in this simulation is obtained when C=2 mm.

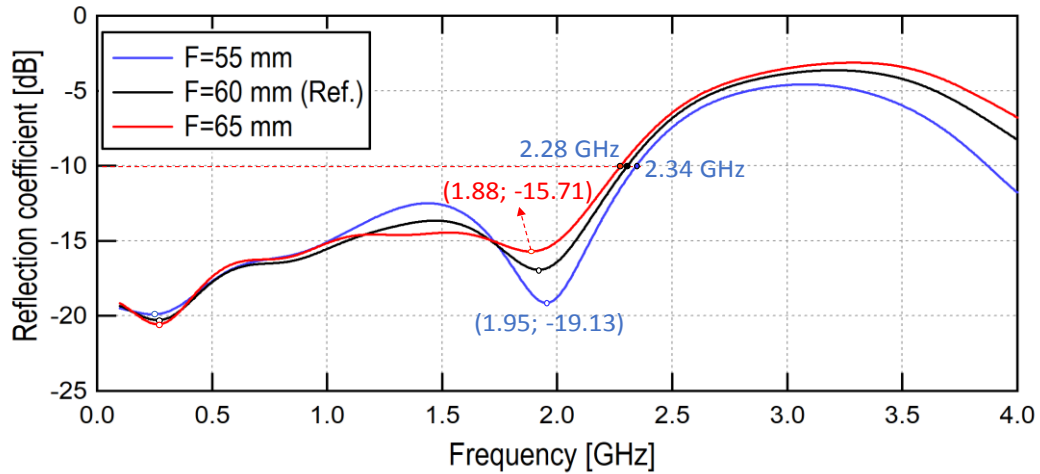


Figure 5. Reflection coefficient of the modified microstrip antenna with length of ground plane (F) of 55 mm, 60 mm, and 65 mm

Figure 5 and Table 3 demonstrate the correlation between varying lengths of the ground plane and the resulting bandwidth, reflection coefficient, and resonance frequency. As the length of the ground plane increases, both the bandwidth and the resonant frequency decreases, while the reflection coefficient slightly improves. Consequently, the microstrip antenna with the shortest ground plane length (F = 55 mm) achieves the largest bandwidth of 2.34 GHz and the lowest reflection coefficient ($\Gamma = -19.13$ dB) at a resonance frequency of 1.95 GHz, which falls within the frequency range of PD occurrence. This result signifies an improvement in bandwidth compared to the initial design

Table 3. S_{11} parameter simulation results of varying length of ground plane (F)

Length of Ground Plane [mm]	Bandwidth [GHz]	Reflection Coefficient Γ [dB]	Resonance frequency [GHz]
55 mm	2.343	-19.133	1.953
60 mm [ref.]	2.30	-20.28, -16.93	0.26, 1.92
65 mm	2.276	-15.707	1.882

2-4- Modification of Feed (H)

The feed width, denoted as H in Figure 2, is the last dimension that yields different optimized results. The initial value of 2 mm was modified to 1 mm and 3 mm. The simulation results for the S_{11} parameter are presented in Figure 6 and Table 4.

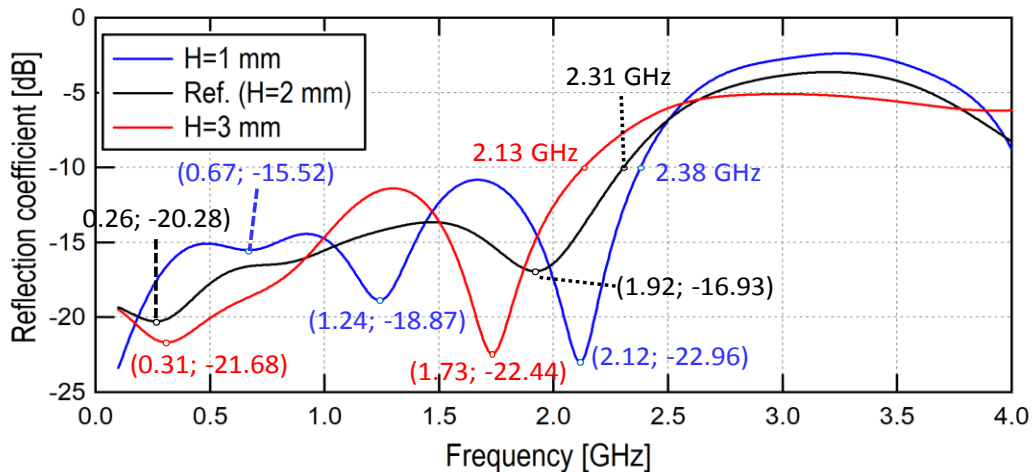


Figure 6. Reflection coefficient of the modified microstrip antenna with feed width (H) of 1 mm, 2 mm, and 3 mm

Table 4. S_{11} parameter simulation results of varying feed width (H)

Feed Width [mm]	Bandwidth [GHz]	Reflection Coefficient Γ [dB]	Resonance frequency [GHz]
1 mm	2.38	-15.52, -18.87, -22.96	0.67, 1.24, 2.12
2 mm [ref.]	2.30	-20.28, -16.93	0.26, 1.92
3 mm	2.13	-21.68, -22.44	0.31, 1.73

Similar to the ground plane length modification, changing the feed width affects the bandwidth. The reflection coefficient decreases as the feed width is reduced, with the largest bandwidth achieved at the smallest feed width of 1 mm. Nevertheless, as shown in Figure 5, small changes in the feed might result in increased reflections. However, this is not a significant issue since the reflections occur at a reflection coefficient below -10 dB. The optimized feed width of 1 mm resulted in the lowest reflection coefficient of -22.96 dB at the resonant frequency of 2.12 GHz, which falls within the frequency range of PD occurrence. Finally, Table 5 provides a summary of the bandwidth, reflection coefficient, and resonant frequency for each optimized dimension of the microstrip antenna.

Table 5. Summary of microstrip antenna characteristics for each optimized dimension

Modified Dimension	Bandwidth [GHz]	Reflection Coefficient Γ [dB]	Resonance frequency [GHz]
Initial design	2.30	-20.28, -16.93	0.26, 1.92
Length of arms (A=55 mm)	2.39	-20.80	0.27
Length of ground plane (F=55 mm)	2.34	-19.13	1.95
Feed (H=1 mm)	2.38	-15.52, -18.87, -22.96	0.67, 1.24, 2.12

3- Antenna Fabrication and Characterization

3-1-Antenna Fabrication

The microstrip antenna was designed with optimized dimensions for the length of arms, length of the ground plane, and feed. The optimized design, along with the initial design, are fabricated on PCBs made of an FR4-epoxy substrate. The antennas are fabricated using the image photo transfer method, which can produce PCB tracks with high accuracy, up to 0.254 mm [22]. This method requires negative films (dry film photoresist/photosensitive film) as the transfer image media, as shown in Figure 7. Figure 8 depicts the fabrication result of the initial design of modified microstrip antenna on an FR4-epoxy PCB.

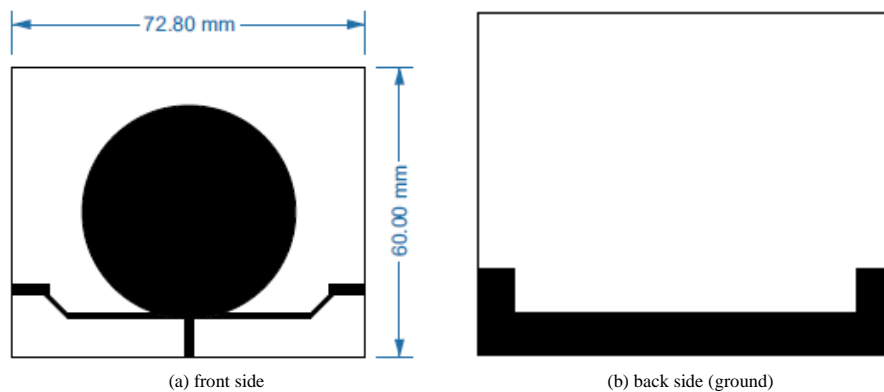


Figure 7. Negative films of the initial design of modified microstrip antenna

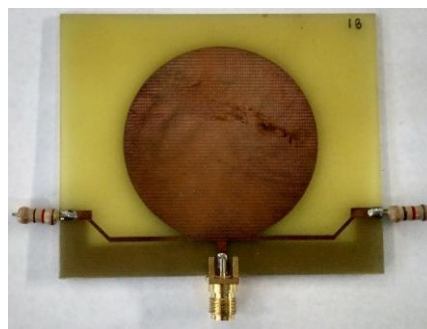


Figure 8. Fabricated initial design of modified microstrip antenna (Antenna 1) on PCB

As simulated in the preceding section, four modified microstrip antennas were fabricated.

- 1) Initial design of modified microstrip antenna (Antenna 1);
- 2) Modified microstrip antenna with optimized length of arms (Antenna 2);
- 3) Modified microstrip antenna with optimized length of ground plane (Antenna 3);
- 4) Modified microstrip antenna with optimized feed (Antenna 4).

3-2- VNA Measurement Results

Figure 9 displays the reflection coefficient characteristics of each fabricated antenna measured using a VNA. Each type of modified antenna, with certain optimized dimensions, is fabricated three times. Thus, the graph in Figure 9 presents the VNA measurement results for the three fabricated antennas (A, B, and C) of the same type (e.g., Antenna 1) in comparison to the simulation results of the reflection coefficient characteristics.

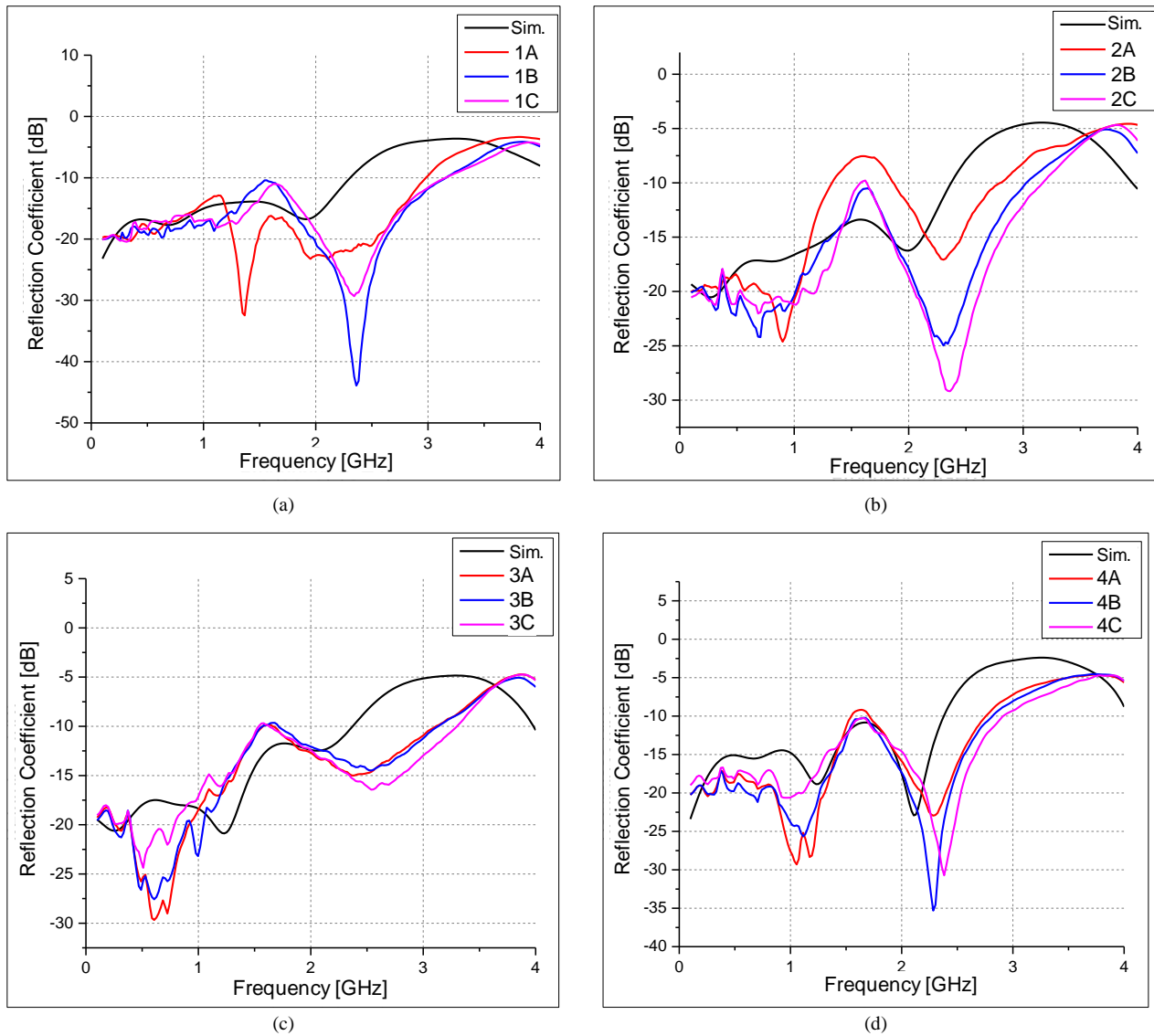


Figure 9. Reflection coefficient characteristics by VNA measurement results of (a) Initial design of modified antenna (Antenna 1), (b) Antenna 2, (c) Antenna 3, and (d) Antenna 4

Table 6 depicts the total bandwidth for each type of the modified microstrip antenna, with a reflection coefficient below -10 dB. These values are obtained from Figure 9 and are compared to the simulation results. The table indicates differences in the total bandwidth between the simulation and three fabricated antenna types. These differences may be attributed to imperfections in the fabrication method, leading to deviations in bandwidth, reflection coefficients, and resonant frequencies, even among antennas of the same type.

Table 6. Total bandwidth of modified microstrip antenna based on VNA measurement results

Antenna types	Total bandwidth [GHz]			
	Antenna 1	Antenna 2	Antenna 3	Antenna 4
Initial design	2.30	2.39	2.34	2.38
Simulation	2.96	2.24	2.99	2.58
Antenna A	3.14	3.02	2.97	2.81
Antenna B	3.14	3.08	3.17	2.90

Only one antenna of each type with the widest overall bandwidth will be used for the PD detection tests and measurements. Table 7 shows the reflection coefficients and their respective resonant frequencies of the modified antennas with the widest total bandwidth for each type, in contrast to the simulation results.

Table 7. Reflection coefficients and resonant frequencies of modified microstrip antenna based on VNA measurement results

Antenna types	Reflection Coefficient [dB]		Resonant Frequencies [GHz]	
	Simulation	VNA	Simulation	VNA
Initial design	-20.28, -16.93	-44.03	0.26, 1.92	2.37
Simulation	-20.80	-29.24	0.27	2.36
Antenna A	-19.13	-24.43	1.95	0.51
Antenna B	-15.52, -18.87, -22.96	-30.90	0.67, 1.24, 2.12	2.39

4- Partial Discharge (PD) Detection Tests

4-1-PD Detection Test Method

To experimentally verify the accuracy of detecting, a partial discharge (PD) detection experiment is conducted using air as the insulation medium. prove if the modified microstrip antennas can detect PD properly with the correct PD pattern. Figure 10 displays the experimental setup for the PD measurement circuit in the laboratory, which includes needle-plane electrodes in air, as depicted in Figure 11.

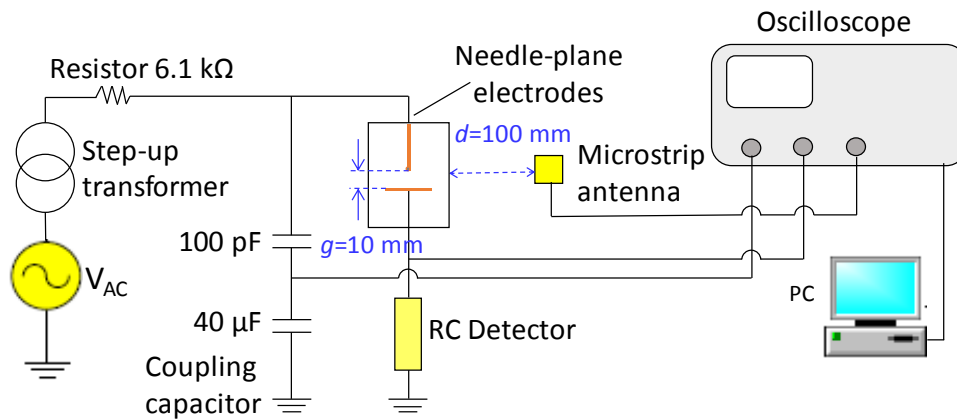


Figure 10. PD detection and measurement circuit

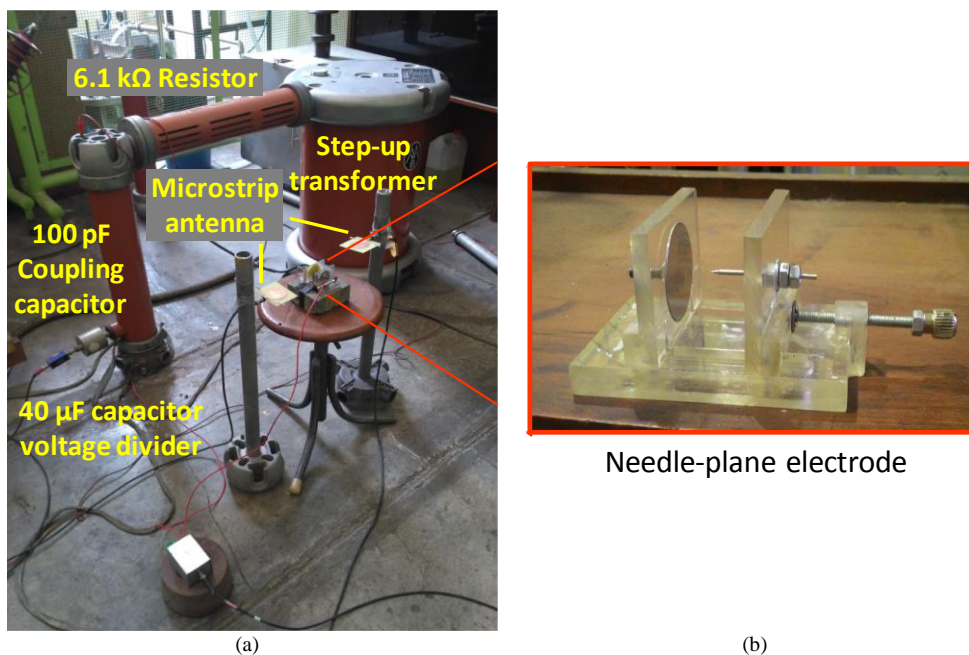


Figure 11. (a) PD detection experimental set up in HV laboratory with (b) PD source using needle-plane electrode

Three kinds of measurement are conducted to evaluate the performance of the modified microstrip antennas in detecting both positive and negative PD, as follows:

- 1) PDIV measurement;
- 2) PD waveform measurement;
- 3) PD phase patterns.

Prior to conducting PD measurements, the background noise is assessed under two conditions: with the power supply deactivated and then activated. This measurement is conducted before antenna is installed or in proximity to the PD sources to determine the background voltage level in millivolts (mV). In the time domain, signals exceeding the background noise level are identified as PD signals. Moreover, the utilization of UHF antennas in an ultrawide frequency range makes them susceptible to interference caused by high-frequency noise. Nevertheless, PD signals exhibit a frequency spectrum that is significantly different from noise. Therefore, in addition to the time-domain background noise measurement, data also can be analyzed in the frequency domain. This enables us to differentiate PD signals that occur beyond the range of frequencies affected by noise.

Subsequently, PD measurements are conducted at different applied voltages. The results of these measurements are discussed in the following sections.

4-2-PDIV Measurement Results

The first measurement aims to determine the negative and positive PDIV, with the results shown in Figure 12. The result indicate that all modified microstrip antennas can detect both negative and positive PD at higher PDIV compared to the RC detector. In addition, it is confirmed that the modified microstrip antennas (Antenna 2, 3, and 4) have lower PDIV than the initial design (Antenna 1), demonstrating higher sensitivity in the antennas with optimized length of arms, length of ground plane, and feed.

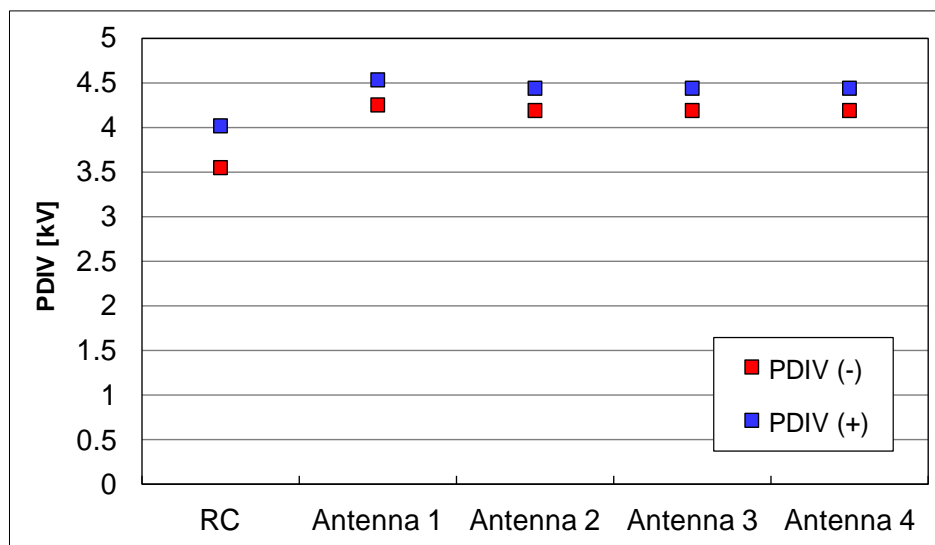


Figure 12. Negative and positive PDIV for each modified microstrip antenna in comparison with RC detector

In the second experiment, the PD measurements are conducted using each modified microstrip antenna at three different applied voltages, i.e., 6 kV, 6.5 kV, and 7 kV. These results are then compared to the measurements obtained by the RC detector. The voltage range used for measuring PD spans from 4.3 kV for the negative PDIV to 4.5 kV for the positive PDIV, with a maximum breakdown voltage of approximately 8 kV. PD pulses are recorded around the PDIV at 5 kV, but the number of pulses was insufficient to form a Phase-Resolved Partial Discharge (PRPD) pattern. Consequently, the starting PD measuring voltage is set at 6 kV, followed by 6.5 kV, and a maximum applied voltage of 7 kV.

Figure 13 illustrates the increasing negative PD magnitudes as applied voltages increase, compared with background noise measurements detected by the RC detector and Antennas 1–4. The graph shows that the acquired PD magnitudes consistently exceed the levels of background noise for each sensor, within a range of applied voltages from 6 to 7 kV. Furthermore, the graph clearly shows a steady rise in PD amplitude, as measured by each antenna, with an increase in applied voltage. While the differences in measurement results are not significant, the PD amplitude obtained from Antenna 2, which is a modified microstrip antenna with optimized length of arms, is greater than the PD amplitudes obtained from the other modified microstrip antennas with different optimized parameters.

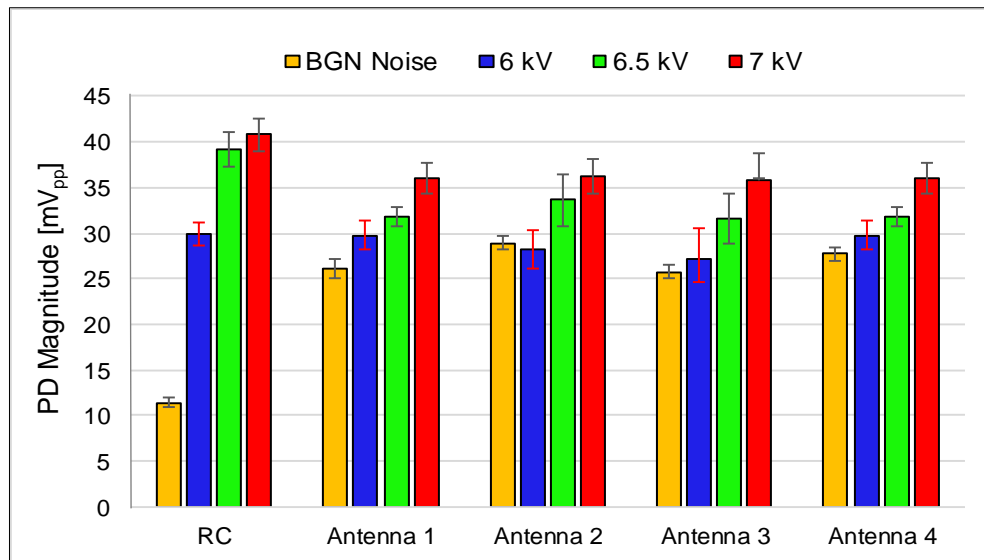


Figure 13. Negative PD amplitude and background noise measurement results by each modified microstrip antenna compared to RC detector at various applied voltages

Figures 14 and 15 present examples of PD signal waveforms measured by the RC detector and all modified microstrip antennas at an applied voltage of 6 kV for negative PD and positive PD, respectively. The figures show that each modified microstrip antenna can detect both negative and positive PD. It is also evident from Fig. 14 that the amplitude of positive PD measured by each modified microstrip antenna is consistently larger than the amplitude of negative PD at the same applied voltage. This suggests that all modified microstrip antennas with different optimized parameters can properly detect negative and positive PD.

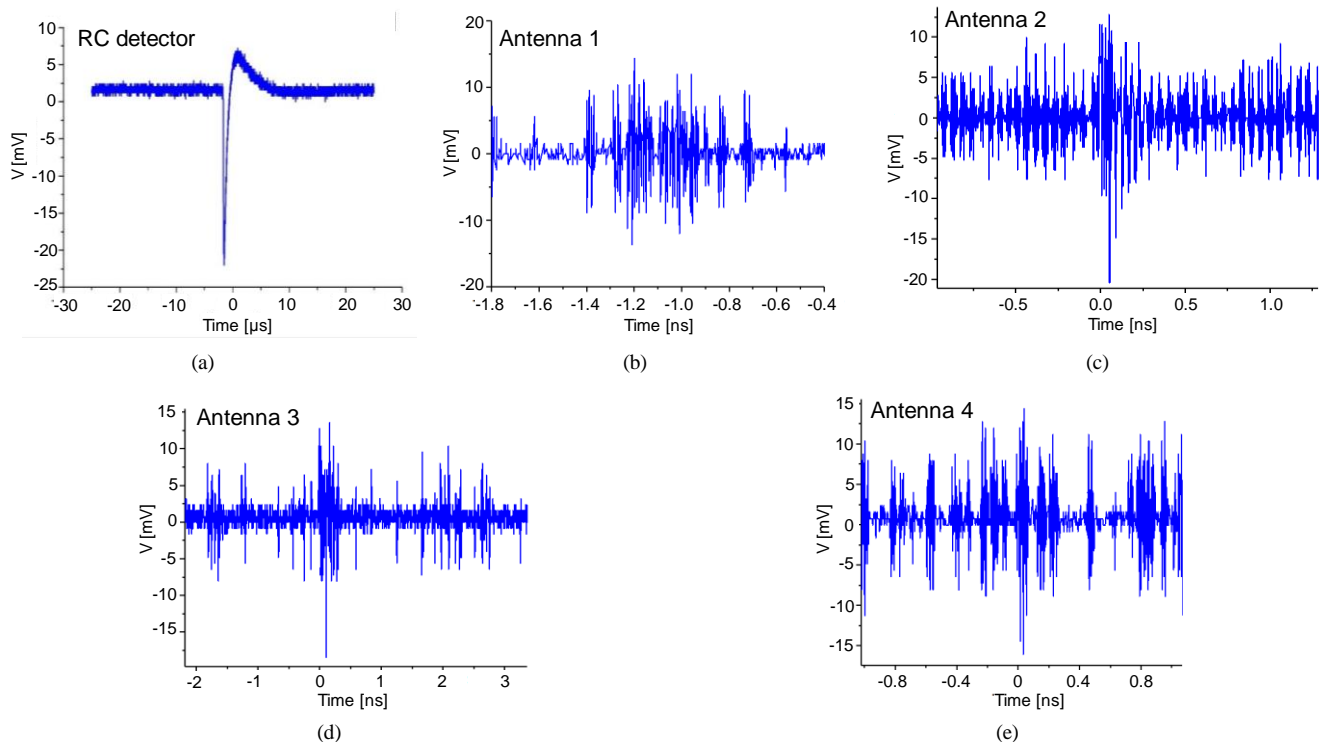


Figure 14. Negative PD signals measured by (a) RC detector, (b) Antenna 1, (c) Antenna 2, (d) Antenna 3, and (e) Antenna 4 at 6 kV applied voltage

The results also show that the magnitudes of the PD measured by the antennas are consistently lower than those identified by the RC detector. This difference is due to the fact that the antennas indirectly measure PD pulses via electromagnetic waves in the medium (air), resulting in signal attenuation. On the other hand, the RC detector, which is a part of the measuring circuit, directly measures the PD current emanating from the PD source.

For the subsequent experiments, only the results of Antenna 1 (the initial design) and Antenna 2 (the modified microstrip antenna with an optimized length of arms) will be discussed and analyzed. These two antennas, out of the four modified versions, exhibited the largest bandwidth and are considered representative of the enhanced designs. Their

performance will be compared with the direct measurement results obtained by the RC detector. Table 8, Figure 16, and Figure 17 present the experiment results, which include the PD pattern, PD magnitude, and the number of PDs measured against increased applied voltage

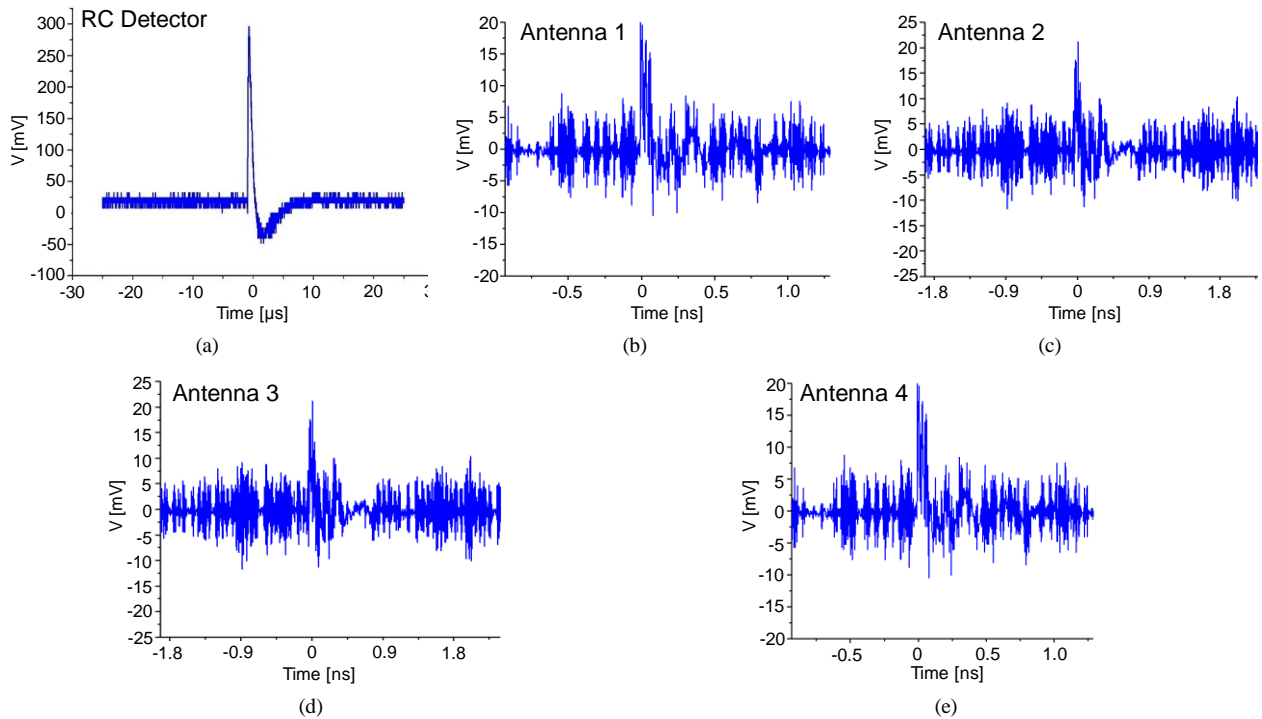


Figure 15. Positive PD signals were measured by (a) RC detector, (b) Antenna 1, (c) Antenna 2, (d) Antenna 3, and (e) Antenna 4 at 6 kV applied voltage

Table 8. PD phase pattern at various applied voltages

Voltage [kV]	RC detector	Antenna 1	Antenna 2
6			
6.5			
7			

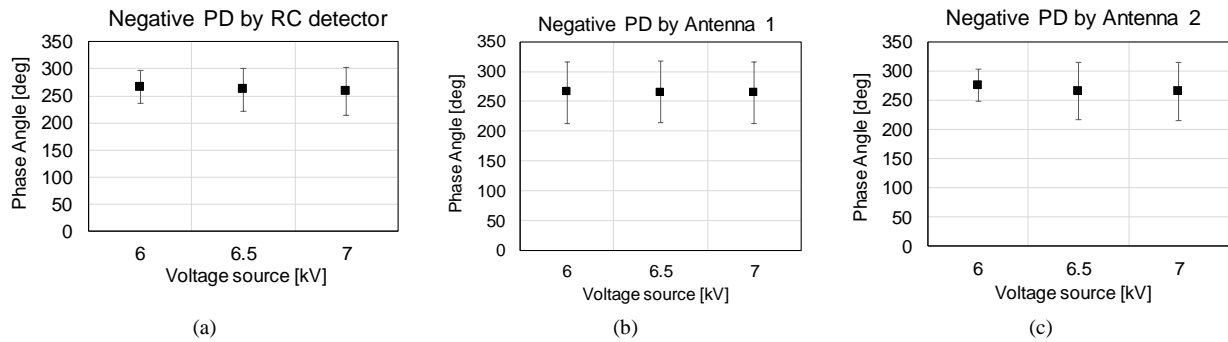


Figure 16. Phase angle of negative PDs measured by (a) RC detector, (b) Antenna 1, and (c) Antenna 2 at various applied voltages

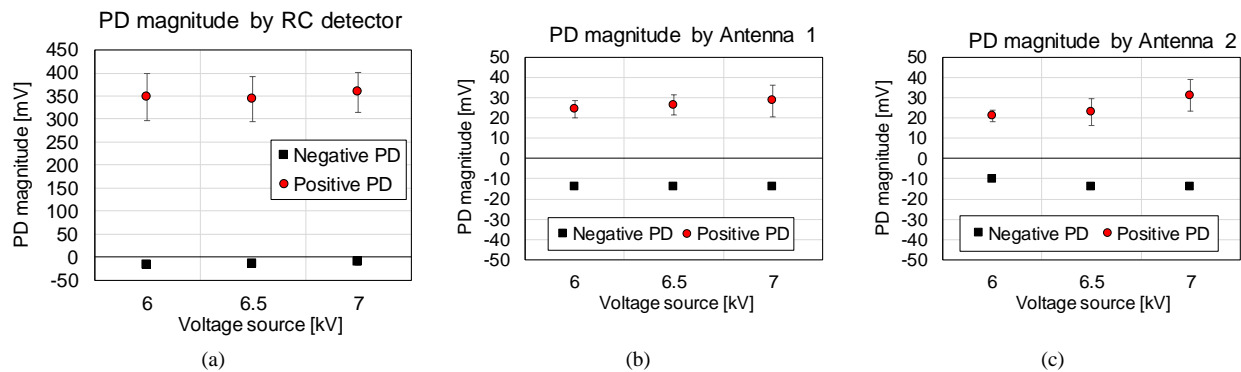


Figure 17. PD magnitude measurement of negative and positive PDs by (a) RC detector, (b) Antenna 1, and (c) Antenna 2 at various applied voltage

Table 8 presents the PRPD pattern, which includes PD measurement results such as phase angle (φ), magnitude (V_{pp}), and number of detected PDs (n). In the needle-plane electrode configuration for PD analysis in air, the initial PD event is a negative discharge that usually occurs at the peak of the negative voltage cycle, with a phase of around 270° . As the applied voltage increases, negative PD pulses appear with smaller magnitudes and higher repetition rates compared to positive PD pulses. When a voltage level exceeds the PDIV, newly occurring negative PD pulses align with the peak of the negative cycle. Existing PD pulses at voltages below the current source, such as PDIV, are positioned at phases lower or higher than the 270° peak. This leads to a scattered phase pattern of PD pulses inside the negative cycle.

Positive PD pulses, on the other hand, occur when the voltage exceeds the positive PDIV and have considerably larger magnitudes compared to their negative counterparts. Consequently, in the PRPD pattern, negative PD plots are distributed across the negative cycle with reduced magnitude, whereas positive PD pulses tend to concentrate near the apex of the positive cycle [22, 23]. Overall, the table also depicts the number of PD occurrences, qualitatively indicated by the number of red dots. The PD phase pattern is obtained within 100 cycles. It is evident from the table that both Antenna 1 and Antenna 2 are capable of detecting both negative and positive PDs in the correct pattern, which is comparable to the pattern detected by the RC detector.

Figures 16-a to 16-c provide a comprehensive comparison of the phase angle of PDs recorded at different applied voltages by the RC detector, Antenna 1 (the initial design), and Antenna 2 (modified antenna with optimized length of arms), respectively. In terms of phase angle, Figure 16 shows that both antennas detect negative PDs with an average phase angle of around 260° , which is similar to the phase angles observed by the RC detector. This corresponds to a typical PD pattern resulting from a needle-plane electrode, which usually shows negative PDs with a 270° phase angle [24].

Figures 17-a to 17-c, display the PD magnitude measured by the RC detector, Antenna 1, and Antenna 2, respectively. The results indicate that the PD magnitude detected by Antennas 1 and 2 is similar, in the range of 10-15 mV. However, the increase in PD magnitude with applied voltages measured by Antenna 2 is greater than that measured by Antenna 1, indicating that Antenna 2 has higher sensitivity.

Finally, the number of negative and positive PDs detected by the RC detector, Antenna 1, and Antenna 2, is shown in Figure 18. The chart illustrates that the number of detected PDs for both negative and positive PD rises in correlation with the escalation of applied voltages for all types of PD detectors.

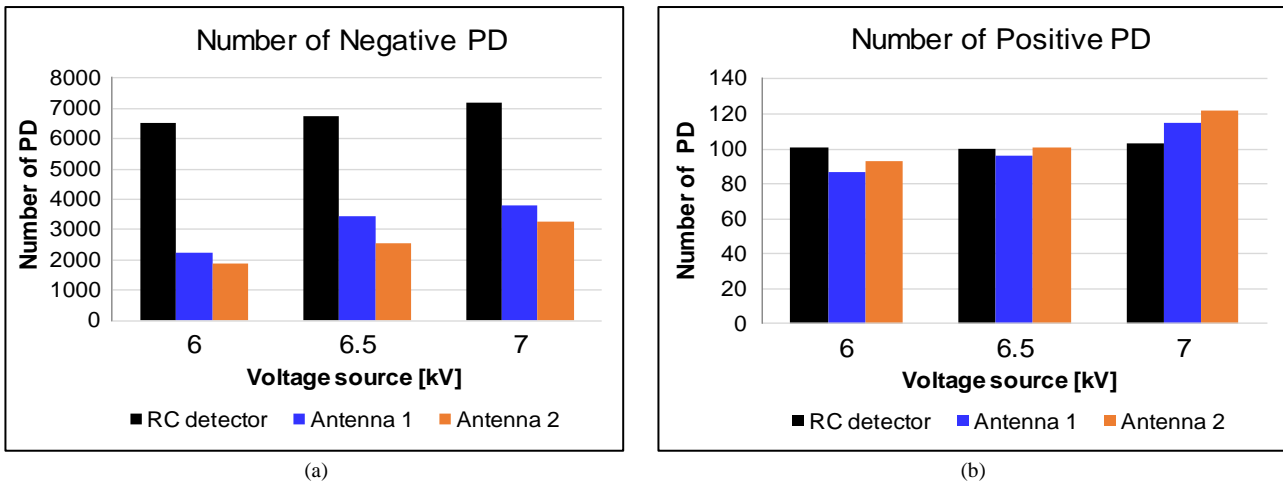


Figure 18. Number of (a) negative and (b) positive PDs detected by RC detector, antenna 1, and antenna 2 at various applied voltage

5- Analysis and Discussion

The modified microstrip antenna was originally based on the design for a surface penetrating radar (SPR) by Simorangkir et al. [20, 21]. This design required an operating frequency range of 50 MHz to 5 GHz. Consequently, their microstrip antenna design successfully attained a very large bandwidth, specifically approaching 5 GHz with certain structural modifications. However, despite using this design as a reference, some structural dimensions were not specified and were thus determined by the authors of this paper, resulting in the reference antenna (initial design) shown in Figure 2. These differences in dimensions could affect antenna performance, particularly the bandwidth, which fell short of reaching 5 GHz.

Our objective was to enhance antenna performance for UWB PD detection in SF₆ gas within the range of 300 MHz to 3 GHz. Previous research on PD detection in GIS utilized a rounded-edge bowtie antenna with a maximum bandwidth of only 450 MHz [7]. Compared to other antennas suitable for installation in GIS dielectric windows [7, 13], the current modified microstrip antenna achieves a significantly larger bandwidth of up to 3.14 GHz. On average, the bandwidth of the current modified microstrip antenna is 6 to 7 times wider than that of the previously researched modified bowtie antenna.

The optimization of the current microstrip antenna design has shown slight improvements in performance in terms of bandwidth and resonant frequency when compared to the initial design (Antenna 1 in Tables 6 and 7). The largest bandwidth, 2.39 GHz (for a reflection coefficient of less than -10 dB), is achieved by the modified microstrip antenna with optimized length of arms. It has reflection coefficients of -20.8 dB, -18.25 dB, -14.62 dB at resonant frequencies of 273 MHz, 1.25 GHz, and 2.01 GHz, respectively. These results indicate that the modified microstrip antennas with optimized length of arms and other dimensions, as shown in Tables 6 and 7, have improved bandwidth of 2–3 GHz, covering the frequency range of PD signals in SF₆ gas. Additionally, they exhibit low reflection coefficients at several resonant frequencies up to around 2 GHz, suggesting high efficiency in absorbing PD signals for enhanced accuracy in measurement results.

Based on the PD measurement data in air shown in Section IV B, both the reference antenna (Antenna 1) and those with optimized dimensions (Antenna 2 to 4) successfully detected and measured PD signals. This is demonstrated by their ability to identify PD with lower negative PDIV in comparison to positive PDIV, as shown in Figures 12 and 13, for all antenna types, including the reference modified microstrip antenna and those optimized for length of arms, length of ground plane, and feed. The fabricated antennas also give correct response to increasing applied voltage during PD measurement, as shown in Figure 13 and Table 8, for both negative and positive PDs. The PD pulse magnitudes measured by the antennas are consistently smaller than those obtained by the RC detector, primarily due to attenuation in the medium. A pC pulse calibrator can be used to determine the actual charge associated with the detected PD pulses. For accurate calibration, the PD pulses detected by both the antenna and the RC detector must occur in the same sequence during simultaneous measurements.

Table 9 also depicts the correct PD pattern measured by all antenna types for PD occurring in air with needle-plane electrodes. This is indicated by negative PDs with a 270° phase angle of applied voltage, corresponding to PDIV and the peak of negative voltage. Table 9 presents a summary of the comparison between the characteristics of the current modified microstrip antenna and those obtained from prior research.

Table 9. Comparison of the current modified microstrip antenna characteristics from previous research

Types of antenna	Bandwidth ($\Gamma < -10$ dB)	Min Γ [dB]	Resonant freq. (GHz)
Cutting-edge modified Circular Microstrip Patch Antenna (CMPA) [22, 23]	0.9~1.4 GHz, 1.6 ~ 4.4 GHz (Total 3.4 GHz)	-31.3	1.3
		-34.6	2.1
		-41.8	2.9
		-27.9	3.6
		-29.3	4.1
Rounded edge modified bowtie antenna [25]	0.45 (1.41~1.86)	-21.80	1.56
Middle-sliced modified bowtie antenna [25]	0.39 (1.26~1.65)	-23.22	1.40
Initial design of modified microstrip antenna (Current work)	3.14 (0 – 3.14)	-20.00	0.26, 0.32
		-19.47	0.51
		-19.87	0.64
		-18.68	0.71, 1.09
		-18.16	0.91
		-15.79	1.27
		-44.03	2.37
Modified microstrip antenna with optimized length of arms (Current work)	3.08 (0~1.59, 1.64 – 3.08)	-21.29	0.32, 0.47, 1.02
		-22.05	0.69
		-20.23	1.17
		-29.24	2.36

The significant characteristic of the currently modified microstrip antennas is their continuously low reflection coefficient ($\Gamma < -10$ dB) over a wide bandwidth, ranging from a few kHz to over 3 GHz. This feature is infrequently observed in our own or other groups' previous research on other types of PD UHF sensors. For example, our previous bowtie antennas had bandwidths of only 450 MHz (1.41-1.86 GHz) and 320 MHz (1.39-1.71 GHz), for the rounded edge bowtie antenna and the middle-sliced bowtie antenna, respectively [7]. Uwiringiyimana et al. [26] designed a different shape of modified CPMA with a total bandwidth of 3.4 GHz, however the bandwidth where its reflection coefficient of less than -10 dB only begins at 0.9 GHz, which makes it less effective for detecting PD in the frequency range below 1 GHz.

In contrast, the modified microstrip antennas presented in this paper exhibit consistent and optimal performance throughout a broad frequency range of approximately 3 GHz. Compared to other types of UHF sensors, this ensures more accurate detection of PD signals in SF₆ gas across all frequency ranges. In addition, the ultrawide bandwidth of these modified microstrip antennas enables them to accurately measure PD in different media. This includes the low-frequency range ($f < 20$ MHz) in air, ($f < 200$ MHz) in oil, and ($0.3 < f < 3$ GHz) in SF₆ gas. This capability is very beneficial for measuring PD using equipment with limited bandwidth.

Regarding reflection coefficient, the current modified microstrip antenna (Antenna 1) exhibits excellent performance at higher operating frequencies (2–3 GHz), with a reflection coefficient of -44.03 dB at a resonant frequency of 2.37 GHz. This is significantly lower than the modified CPMA [26] and nearly twice as low as the modified bowtie antennas [7].

6- Conclusions

Design and modification on a UWB microstrip antenna in this research have resulted in improved bandwidth, where the fabricated initial design of the modified antenna has a total bandwidth of 3.14 GHz, and the fabricated modified microstrip antenna with optimized length of arms has a total bandwidth of 3.08 GHz. The lowest reflection coefficients of the modified reference microstrip antenna and the modified microstrip antenna with optimized length of arms are -44.03 dB at 2.37 GHz resonant frequency and -29.24 dB at 2.36 GHz resonant frequency, respectively.

The main findings of our research indicate that the modified microstrip antenna achieves a bandwidth of 3.1 GHz, nearly seven times wider than our previous modified bowtie antennas. This significant improvement provides a comprehensive range for PD signal detection. Additionally, the modified microstrip antenna exhibits a continuously and constantly low reflection coefficient (< -10 dB) that starts from a few kHz (low frequency) until 3 GHz, where Antenna 1 and Antenna 2 yield 116% and 112% coverage of the UHF band (0.3 to 3 GHz), respectively. These characteristics allow these antennas to operate with high efficiency for detecting and measuring PD in the UHF range, i.e., in SF₆ gas insulation medium, as well as in the low-frequency range, e.g., in air insulation medium. Furthermore, our modified microstrip antenna maintains a compact size of 60×73 mm², fitting within the less than 100 mm length requirement of GIS dielectric windows, presenting a notable advantage.

The performance of the fabricated modified microstrip antennas is then validated by PD measurement experiments in the laboratory. The results show that both the initial design of the modified microstrip antenna and the modified

microstrip antenna with an optimized length of arms can detect PD signals in air successfully. Both antennas can detect negative PD signals at lower PDIV than the positive ones, are well-response to the increased voltage during PD measurement seen from the increased detected PD magnitude, and are able to detect PD signals with the correct PD pattern following the PD pattern in air with a needle-plane electrode.

Nevertheless, due to limitations in the laboratory, the validation of this antenna's performance in detecting and measuring PD signals in SF₆ gas insulation medium has not been conducted. It will be one of our future works. It is also suggested to compare the PD measurement results by the current modified microstrip antennas with the measurement results by other types of antennas.

Finally, the presently designed microstrip antenna exhibits adequate bandwidth for detecting the majority of PD within SF₆ gas, spanning from 0.3 to 3 GHz. However, certain limitations exist, notably the inability to capture PD signals at higher frequencies and the relatively low magnitude of detected PD signals when compared to an RC detector. Our future works will also focus on refining this microstrip antenna design through combinations of various optimized dimensions, aiming to expand the bandwidth. Additionally, we plan to enhance detection capabilities by incorporating an amplifier into the detection circuit to improve gain.

7- Declarations

7-1- Author Contributions

Conceptualization, U.K.; methodology, U.K., and Y.M.H.; software, Y.M.H.; validation, Y.M.H. and U.K.; formal analysis, Y.M.H.; investigation, Y.M.H.; resources, U.K.; data curation, U.K. and R.; writing—original draft preparation, R.; writing—review and editing, R.; visualization, Y.M.H. and R.; supervision, U.K.; project administration, U.K.; funding acquisition, U.K. All authors have read and agreed to the published version of the manuscript.

7-2- Data Availability Statement

The data presented in this study are available in the article.

7-3- Funding

This work is financially supported in parts by Research, Community Service and Innovation Program (P2MI) funded by School of Electrical Engineering and Informatics (STEI), Institut Teknologi Bandung (ITB), Indonesia, and by program Hibah Dosen Tidak Tetap Peneliti 2024 managed by The Directorate for Multidisciplinary Science and Technology Implementation (DPITM), ITB, financially from the DAPT EQUITY Program, Indonesia Endowment Fund for Education (LPDP), the Ministry of Finance, Indonesia.

7-4- Institutional Review Board Statement

Not applicable.

7-5- Informed Consent Statement

Not applicable.

7-6- Conflicts of Interest

The authors declare that there is no conflict of interest regarding the publication of this manuscript. In addition, the ethical issues, including plagiarism, informed consent, misconduct, data fabrication and/or falsification, double publication and/or submission, and redundancies have been completely observed by the authors.

8- References

- [1] Stone, G. C., Culbert, I., Boulter, E. A., & Dhirani, H. (2014). *Electrical Insulation for Rotating Machines*, John Wiley & Sons, Hoboken, United States. doi:10.1002/9781118886663.
- [2] Genutis, D. A. (2006). *Electrical Equipment Condition Assessment Using On-Line Solid Insulation Sampling*. Neta World, United States, 1-5.
- [3] Suwarno. (2016). Partial discharge in high voltage insulating materials. *International Journal on Electrical Engineering and Informatics*, 8(1), 147–163. doi:10.15676/ijeii.2016.8.1.11.
- [4] Han, X., Li, J., Zhang, L., Pang, P., & Shen, S. (2019). A Novel PD Detection Technique for Use in GIS Based on a Combination of UHF and Optical Sensors. *IEEE Transactions on Instrumentation and Measurement*, 68(8), 2890–2897. doi:10.1109/TIM.2018.2867892.
- [5] Sinurat, M. S., & Khayam, U. (2019). Characteristic of PD Phase Patterns, PD Pulse Sequence Patterns and PD Frequency Spectrum in Air Insulation Measured by RC Detector. In *2019 2nd International Conference on High Voltage Engineering and Power Systems (ICHVEPS)*, 1-6. doi:10.1109/ICHVEPS47643.2019.9011091.

- [6] Rodrigo-Morz, A., Muñoz, F. A., & Castro-Heredia, L. C. (2019). A novel antenna for partial discharge measurements in GIS based on magnetic field detection. *Sensors (Switzerland)*, 19(4), 1–17. doi:10.3390/s19040858.
- [7] Rozi, F., & Khayam, U. (2015). Development of loop antennas for partial discharge detection. *International Journal on Electrical Engineering and Informatics*, 7(1), 29. doi:10.15676/ijeei.2015.7.1.3.
- [8] Judd, M. D., Farish, O., Pearson, J. S., & Hampton, B. F. (2001). Dielectric windows for UHF partial discharge detection. *IEEE Transactions on Dielectrics and Electrical Insulation*, 8(6), 953–958. doi:10.1109/94.971451.
- [9] Gharehpetian, G. B., Karami, H., & Ahmadi, S.-A. (2023). Syntactic aperture radar imaging. *Power Transformer Online Monitoring Using Electromagnetic Waves*, 179–246, Academic Press, Cambridge, United States. doi:10.1016/b978-0-12-822801-2.00003-3.
- [10] Mahmoodi, M., Abadi, S. M. N. R., Karami, H., Hejazi, M. A., & Gharehpetian, G. B. (2020). Design and implementation of dielectric windows for detection of radial deformation of HV transformer winding using radar imaging. *IET Science, Measurement & Technology*, 14(4), 478–485. doi:10.1049/iet-smt.2018.5485.
- [11] Li, J., Jiang, T., Cheng, C., & Wang, C. (2013). Hilbert fractal antenna for UHF detection of partial discharges in transformers. *IEEE Transactions on Dielectrics and Electrical Insulation*, 20(6), 2017–2025. doi:10.1109/TDEI.2013.6678849.
- [12] Do Nascimento Cruz, J., Serres, A. J. R., De Oliveira, A. C., Xavier, G. V. R., De Albuquerque, C. C. R., Da Costa, E. G., & Freire, R. C. S. (2019). Bio-inspired printed monopole antenna applied to partial discharge detection. *Sensors (Switzerland)*, 19(3), 1–15. doi:10.3390/s19030628.
- [13] Azam, S. M. K., Othman, M., Illias, H. A., Abdul Latef, T., Tariqul Islam, M., & Fadzil Ain, M. (2023). Ultra-high frequency printable antennas for partial discharge diagnostics in high voltage equipment. *Alexandria Engineering Journal*, 64, 709–729. doi:10.1016/j.aej.2022.11.026.
- [14] Lozano-Claros, D., Custovic, E., & Elton, D. (2016). Two planar antennas for detection of partial discharge in gas-insulated switchgear (GIS). *4th IEEE Conference on Communication, Networks and Satellite, COMNESTAT 2015 - Proceedings*, 8–15. doi:10.1109/COMNETSAT.2015.7434301.
- [15] Azam, S. M. K., Othman, M., Illias, H. A., Latef, T. A., Mahadi, W. N. L. W., Fahmi, D., Hossain, A. K. M. Z., & Ain, M. F. (2023). Planar Sensor for Noise Cancellation during Partial Discharge Detection in Open Substation. *IEEE Sensors Journal*, 23(14), 15552–15562. doi:10.1109/JSEN.2023.3279861.
- [16] Yadam, Y. R., Ramanujam, S., & Arunachalam, K. (2023). Study of Polarization Sensitivity of UHF Sensor for Partial Discharge Detection in Gas Insulated Switchgear. *IEEE Sensors Journal*, 23(2), 1214–1223. doi:10.1109/JSEN.2022.3224475.
- [17] Dhara, S., Koley, C., & Chakravorti, S. (2024). An Ultrawideband Partial Discharge Sensor for High-Voltage Power Transformers. *IEEE Sensors Journal*, 24(10), 16261–16269. doi:10.1109/JSEN.2024.3383064.
- [18] Shu, Z., Wang, W., Yang, C., Guo, Y., Ji, J., Yang, Y., Shi, T., Zhao, Z., & Zheng, Y. (2023). External Partial Discharge Detection of Gas-Insulated Switchgears Using a Low-Noise and Enhanced-Sensitivity UHF Sensor Module. *IEEE Transactions on Instrumentation and Measurement*, 72, 3518210. doi:10.1109/TIM.2023.3277980.
- [19] Pramudita, A., Kurniawan, A., & Suksmono, A. B. (2007, June). Modified dipole antenna for UWB SFCW-GPR. In *Proceedings of the International Conference on Electrical Engineering and Informatics (ICEEI'07)*, 17-19 June, 2007, Bandung, Indonesia.
- [20] Simorangkir, R. B. V. B., & Munir, A. (2011). Numerical design of ultra-wideband printed antenna for surface penetrating radar application. *Telkomnika*, 9(2), 341–350. doi:10.12928/telkomnika.v9i2.706.
- [21] Simorangkir, R. B. V. B. (2010). Compact 50-5000 MHz UWB microstrip antenna for SFCW GPR application. Master Thesis, Institut Teknologi Bandung, Bandung, Indonesia. (In Indonesian).
- [22] Hikita, M., Yamashita, H., Kato, T., Hayakawa, N., Ueda, T., & Okubo, H. (1994). Electromagnetic spectrum caused by partial discharge in air under ac and dc voltage application. *Proceedings of the IEEE International Conference on Properties and Applications of Dielectric Materials*, 2, 570–573. doi:10.1109/icpadm.1994.414074.
- [23] Ra, N., & Khayam, U. (2015). Partial discharge measurement of 4 types of electrodes configuration in air insulation using high frequency current transformer sensor. In *Proceedings of the Joint International Conference on Electric Vehicular Technology and Industrial, Mechanical, Electrical and Chemical Engineering*, 100-105. doi:10.1109/ICEVTIMECE.2015.7496667.
- [24] Yulistya Negara, I. M., Fahmi, D., Asfani, D. A., Satriyadi Hernanda, I. G. N., Soebagio, J. C., & Yulistika Siahaan, V. (2020). Characteristics of Partial Discharge Inception Voltage Patterns Using Antenna in Air Insulation. *ICITEE 2020 - Proceedings of the 12th International Conference on Information Technology and Electrical Engineering*, 263–268. doi:10.1109/ICITEE49829.2020.9271773.
- [25] Khayam, U., & Suryandi, A. A. (2023). Design of Bowtie Antenna with Rounded Edge and Middle-Sliced Modifications for UHF Partial Discharge Sensor. *IEEE Access*, 11, 22822-22834. doi:10.1109/ACCESS.2023.3252006.
- [26] Uwiringiyimana, J. P., Khayam, U., & Montanari, G. C. (2022). Design and implementation of ultra-wide band antenna for partial discharge detection in high voltage power equipment. *IEEE Access*, 10, 10983-10994. doi:10.1109/ACCESS.2022.3144416.